Article

Activity Characteristic of the Two Buried Faults in Zhongwei Basin along the Northeastern Margins of Tibetan Plateau, China, by Means of Shallow Seismic and Composite Drilling Section Exploration

Chao Liu *[ID], Qiyun Lei, Peng Du, Zhiqun Wu, Zeshan Li, Sihan Yu, Shun Yang [ID] and Yin Wang

Earthquake Agency of Ningxia Hui Autonomous Region, Yinchuan 750001, China
* Correspondence: liuchao0426@126.com

Abstract: By using shallow seismic exploration, composite drilling section exploration and sample dating test, we have obtained precise positions, burial depths of uppermost point and activity characteristics of Hetan-Guotan buried fault and Zhenjing-Zhenbei buried fault in Zhongwei Basin. The results show that the latest active period of Hetan-Guotan buried fault is the middle-late Middle Pleistocene, and the latest active period of Zhenjing-Zhenbei buried fault is the Early and Middle Pleistocene. The two buried faults became inactive at the end of the Middle Pleistocene and have been inactive since the Late Pleistocene.

Keywords: the northeastern margins of Tibetan Plateau; Zhongwei Basin; buried faults; activity characteristic

1. Introduction

Earthquakes in plain or basin areas have resulted in extensive damage and heavy casualties; for example, the 1739 *M*8.0 Yinchuan earthquake in China [1], the 1976 *M*7.8 Tangshan earthquake in China [2] and the 1999 *M*7.4 Izmit earthquake in Turkey [3]. A great number of the world's earthquake disaster surveys indicate that active faults are the fundamental cause of earthquakes [4]; however, most of active faults in plain or basin areas are buried under the ground. Compared to the active faults on the surface, detecting buried faults is one of the key and difficult points in active tectonics. A buried fault is one that is hidden by loose Quaternary sediments and is difficult to observe because it has no trace on the surface [5]. Discovering a buried fault and identifying its activity characteristic are of great significance for reducing earthquake damage; however, questions remain over the effective methods to use to complete those studies.

In the 1970s, the southern section of the San Andreas Fault was successfully detected by observing the distribution of radon on the surface [6]. Since then, geologists have tried using this method to identify fault zones, which is named "fault gas detection" [7,8]. Since the late 1980s, the exploration of buried faults gradually evolved into multi-means comprehensive quantitative research, such as shallow seismic exploration, composite drilling section exploration, trial trench, sample dating test and so on [9,10]. Multi-method and multi-level innovation mode is formed, which is called "Combined Detection of Layering and Superimposing" [11]. Shallow seismic exploration can be used to identify the location, properties and depth of a buried fault [12–16], mainly using the reflected wave method. In addition, composite drilling section exploration is needed to verify the fault and to obtain activity parameters and sample dating test for further analysis [17–19].

There are two major faults along the northern and northeastern margins of the Tibetan Plateau, which are called Altyn Tagh Fault and Haiyuan Fault, respectively (Figure 1A). The Haiyuan Fault is located in southern Ningxia Hui Autonomous Region (Ningxia for

short). Ningxia overlaps the junction of three large active blocks, the Tibetan Plateau, the Alashan Block and the Ordos Block (Figure 1B). There are many active faults and destructive earthquakes in Ningxia [20,21], which are affected by the relative movements of the three blocks. The Tianjingshan Fault splays eastward off the north side of the Haiyuan Fault, where the 1709 *M*7.5 Zhongwei earthquake produced a left-lateral surface rupture 30~60 km [22]. The Zhongwei Basin lies on the north side of Tianjingshan Fault, the Yellow River passes there. At present, the existence of buried faults in the Zhongwei Basin and their activity characteristics have been considered only rarely, but these issues need to be addressed urgently, which is a possible seismic hazard and a threat to urban security of Zhongwei City.

In this paper, we present the evidence of shallow seismic exploration to indicate the existence of two buried faults in the Zhongwei Basin, which are called the Hetan-Guotan buried fault and the Zhenjing-Zhenbei buried fault. Then, composite drilling section exploration can effectively determine the precise positions of two buried faults and the burial depths of uppermost point. Additionally, we analyze the activity characteristics of buried faults according to the results of sample dating test. The results show that the two buried faults became inactive at the end of Middle Pleistocene and have been inactive since the Late Pleistocene.

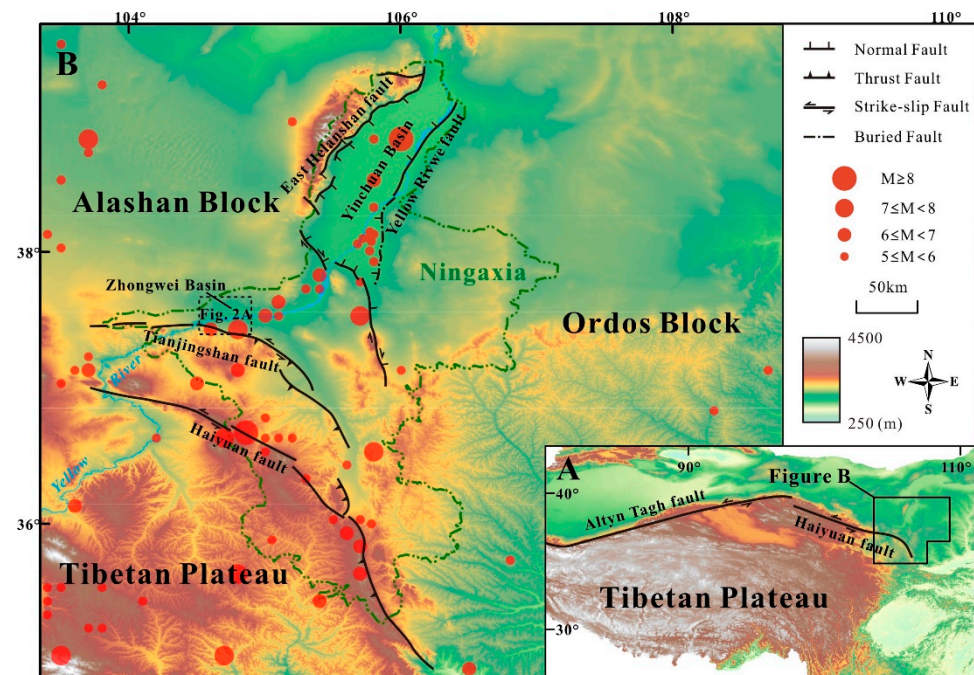**Figure 1.** The tectonic setting of Ningxia. (**A**) Regional tectonic map on the Tibetan Plateau. The black box shows the location of (**B**). (**B**) Topographic and Seismotectonic map of the Ningxia and the surrounding area. Black bold lines in the map represent major active faults. Red solid circles represent the destructive earthquake epicenters (*M* ≥ 5). Dashed black box shows the location of Figure 2A.
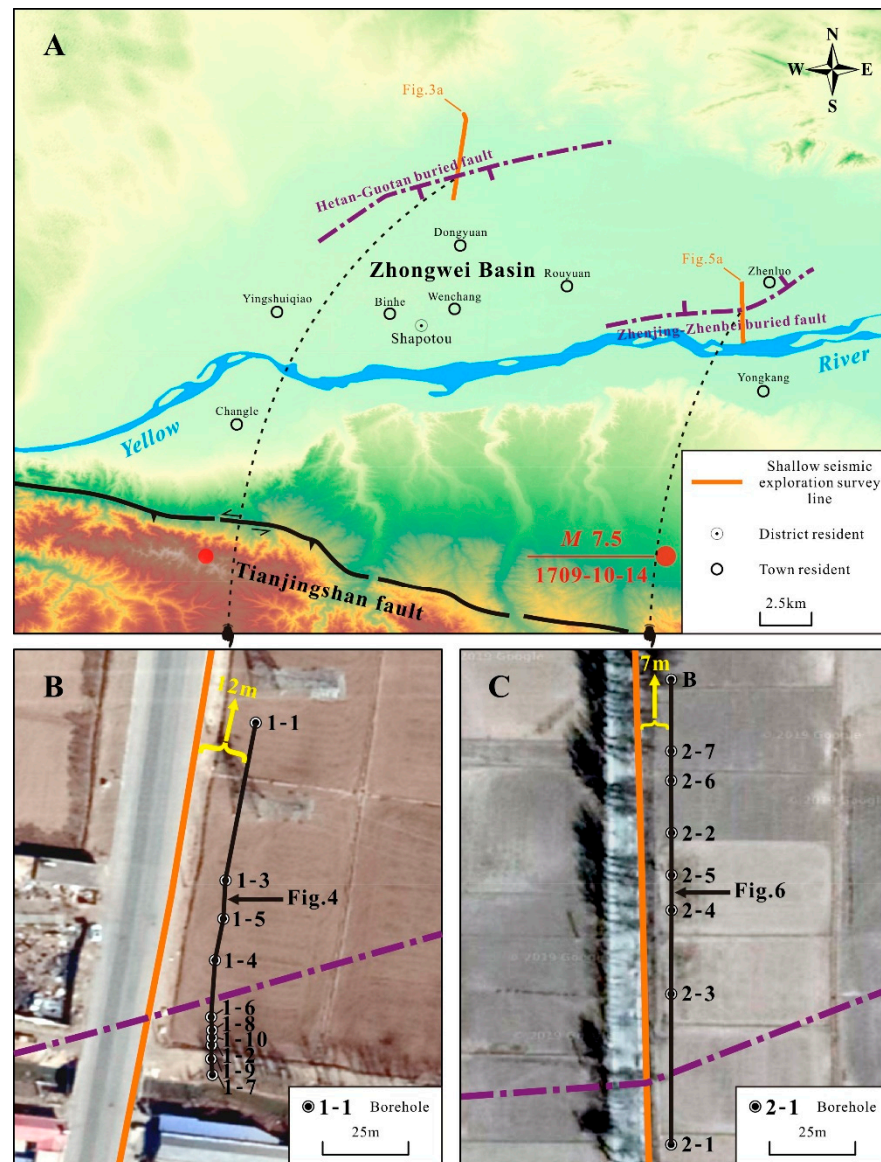
Figure 2. The location of shallow seismic exploration and composite drilling section exploration. (**A**) The distribution of buried faults and shallow seismic survey lines in Zhongwei Basin. The epicenter of the 1709 *M*7.5 earthquake on the Tianjingshan Fault is highlighted. (**B**) The location map of boreholes and composite drilling section exploration (Black bold line) in Xietan Village. (**C**) The location map of boreholes and composite drilling section exploration (Black bold line) in Lizui Village.

2. Methods

2.1. Shallow Seismic Exploration

For shallow seismic exploration, a multiple time coverage reflection wave method was used, which not only helped suppress interference and improve the signal-to-noise ratio of seismic data, but also helped determine the existence and form of the fault via a visual image of the subsurface structure. This shallow seismic data acquisition uses the 428XL digital seismograph produced by Sercel, Nantes, France. All equipment parameters satisfy the requirements of shallow seismic exploration. The seismograph has a high sampling rate, wide recording frequency, large dynamic range and real-time correlation processing of the controllable source data. Two 28 ton vibrators manufactured in the USA, which have strong anti-interference properties, are used to excite seismic waves. Geophone is one of the most important components of the seismic acquisition system. The natural frequency of the geophone used in this acquisition is 60 Hz. Processing of seismic data is conducted

with the Focus software package. The data processing methods mainly include format conversion and data decompiling, de-noising before superposition, deconvolution, statics correction, dynamic correction, common midpoint point (CMP) stacking, inverse filtering after superposition and so on. In the survey, we completed Xietan Village's Survey Line and Lizui Village's Survey Line (location shown in Figure 2A), 4.22 km and 3.0 km, respectively. The observational system and acquisition parameters of seismic data are listed in Table 1. Through two shallow seismic exploration profiles, the locations and properties of two buried faults in the range of the control line were identified and the depths of uppermost points were found. These shallow seismic profiles lay a solid foundation for the detection of buried faults.

Table 1. The observational system and acquisition parameters of seismic data.

Survey Line	Observational System				Geophone Frequency/Hz	Acquisition Parameters		Length/m
	Geophone Interval/m	Minimum Offset/m	Receiving Channels	Fold Number		Sampling Interval/ms	Record Length/s	
Xietan Village	2	0	300	30	60	0.5	2	4220
Lizui Village	3	0	341	34	60	0.5	2	3000

2.2. Composite Drilling Section Exploration

Based on the shallow seismic exploration, we set up two rows of drillings crossing Hetan-Guotan buried fault and Zhenjing-Zhenbei buried fault at Xietan Village and Lizui Village, respectively. The composite section exploration in Xietan Village (location shown in Figure 2A,B) was used to detect the Hetan-Guotan buried fault, and the composite section exploration in Lizui Village (location shown in Figure 2A,C) was used to detect the Zhenjing-Zhenbei buried fault. During the construction, the "folding method" is used to approach the positioning fault from the outside to the inside [23], emphasizing dynamic construction and dynamic analysis. The position of the fault is found through continuous trials. When the sediment particles were small (e.g., clay and sand), the rigs were able to lift out almost all the sediments in the hole, approximately 2 m at a time. When the drilling sediment particles were large (e.g., gravel), the drilling rigs used equidistant interval sampling, taking a sample approximately 0.3 m every 2 m. Tapeline is used to measure drill pipe and core length. The minimum scale of the tapeline is 1 cm, and the measurement error is less than 1 cm. Thus, the number on the centimeter scale is certain and significant. The drill pipe is measured at intervals of 30 m to correct the borehole depth. These ensure that not only the core recovery rate, but also the error in the depth of each borehole is less than 10 cm. It should be noted that since the Middle Pleistocene, the strata have been eroded by the pebble and gravel of Yellow River, and the dating results are relatively old, which makes it impossible to accurately obtain the deposition rate. Therefore, it is very difficult to evaluate the depth and date of the uppermost point by using the deposition rate.

2.3. Sample Dating Test

We immediately collected samples from the drilling sediments. Both ^{14}C and Optically Stimulated Luminescence (OSL) samples should be collected. However, it was difficult to collect ^{14}C samples from the drill core; therefore, only OSL samples were available for this study. Then, these OSL samples were sent to the Optically Stimulated Luminescence Dating Laboratory of the Institute of Earth Environment, Chinese Academy of Sciences for measurement. The dating results of OSL samples are given in the section of "Sample Dating Test". OSL dating ranges from a few hundred years to a hundred thousand years, with an error of about 5%. Among the 15 samples, 1 sample is within the dating range, so the error is small and the reliability is high. The other 14 samples range in age from 100,000 years to more than 200,000 years, beyond the dating range; therefore, the error is

large but less than 10%. This suggests that the formation is older and was deposited before the late Pleistocene.

3. Activity Characteristic of Hetan-Guotan Buried Fault

3.1. Shallow Seismic Exploration of Xietan Village's Survey Line

The shallow seismic exploration of Xietan Village's survey line (see Figure 2A) revealed the existence of the Hetan-Guotan buried fault. Geophone interval of Xietan Village's survey line is 2 m and the total length is 4.22 km from south to north. To distinguish the different reflected wave groups in the same time section and to facilitate interpretation, on the section map, we marked the bottom boundary reflection of the Quaternary overburden with T_Q and the bottom boundary reflection of the Neogene with T_N.

Figure 3a presents the preliminary interpretation of Xietan Village's survey lines. In the south of the survey line stake 850 m from the starting point, a series of reflection layers on the section are distributed nearly horizontally and the event of each reflection wave is parallel to each other, which should be the Cenozoic strata with stable structure. At the survey line stake about 1200~3250 m away from the starting point, multiple sets of strong reflections on the section are tilted to the south, with the event T_Q thinning out upwards. In the north of the survey line stake about 3250 m from the starting point, the T_Q and T_N are almost horizontal and the sedimentary strata are thin. The regional geological data indicate that the Neogene strata in this area are unconformably overlying the Carboniferous strata and generally dip to the south. According to the characteristics of the reflected wave group and the faults in the section, we have conducted a preliminary explanation of five faults. The normal fault dipping to the south and locating at the survey line stake about 1200 m away from the starting position is the most reliable. It breaks all stratigraphic reflections of the T_Q and the stratigraphic reflections below, with a distinguishable uppermost point's burial depth of 39~50 m.

3.2. Composite Drilling Section Exploration in Xietan Village

3.2.1. Layout of Boreholes

Based on the shallow seismic exploration of Xietan Village's survey line, we took Xietan Village as a suitable site to perform the composite section exploration in Xietan Village. The specific site of the composite section exploration in Xietan Village is located in Dongyuan Town, northeast of Shapotou District, Zhongwei City (Figure 2A). The site is in the farmland 12 m east of the Xietan Village's survey line (Figure 2B). The NNE direction of the section is nearly parallel to the Xietan Village's survey line. The boreholes intersect at approximately 70° and crossed the Hetan-Guotan buried fault revealed by the shallow seismic exploration. The survey line of Xietan Village indicates that the uppermost point of the fault is 1200 m away from the starting point of the southern end and the fault is inclined to the south. The boreholes are arranged accordingly. The completed section is 100.0 m long, with 10 boreholes in total. The layout of boreholes is shown in Figures 2B and 3b. The maximum and minimum hole pitches are 46.0 m and 1.9 m, respectively, with an average hole pitch of 11.1 m. The cumulative footage is 801.02 m and the maximum and minimum depths of a single borehole are 99.03 m and 26.75 m, respectively.
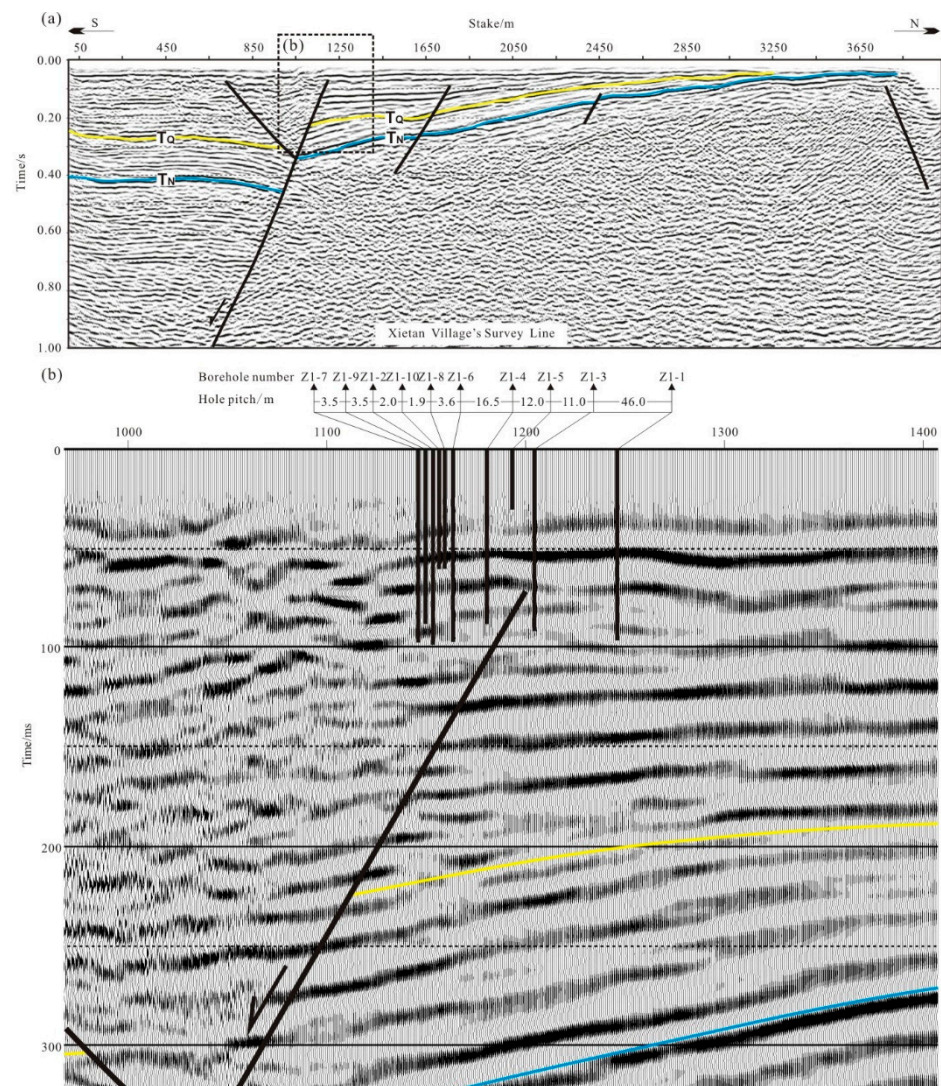
Figure 3. The time profile of Xietan Village's survey line and the layout of boreholes on composite drilling section in Xietan Village. (**a**) A time-stacked section of the shallow seismic line in Xietan Village. Dashed black box shows the location of (**b**). (**b**) The layout of boreholes on composite drilling section in Xietan Village.

3.2.2. Comparison of Stratigraphic Lithology

Based on the core logging of boreholes, we compared the lithological columns of each stratum where the borehole was located. The thick layer of variegated pebble and gravel is distributed over 30 m, and the sand layer and cohesive soil layer alternately appear below the pebble and gravel layer. The color and lithology can be distinguished. There is a significant boundary 50 m below the Earth's surface, dividing the gravelly sand from the cohesive soil. The boundary is broken between Z1-2 and Z1-8, with a fault displacement exceeding 10 m. Due to the rapid lateral variation of the fluvial facies' sedimentary strata, it is difficult to make stratification only by lithology. It is necessary to consider the characteristics of color, stratification and structure to divide the drilled strata of Xietan Village into 6 strata (Figure 4 ①~⑥). The strata from top to bottom are as follows:
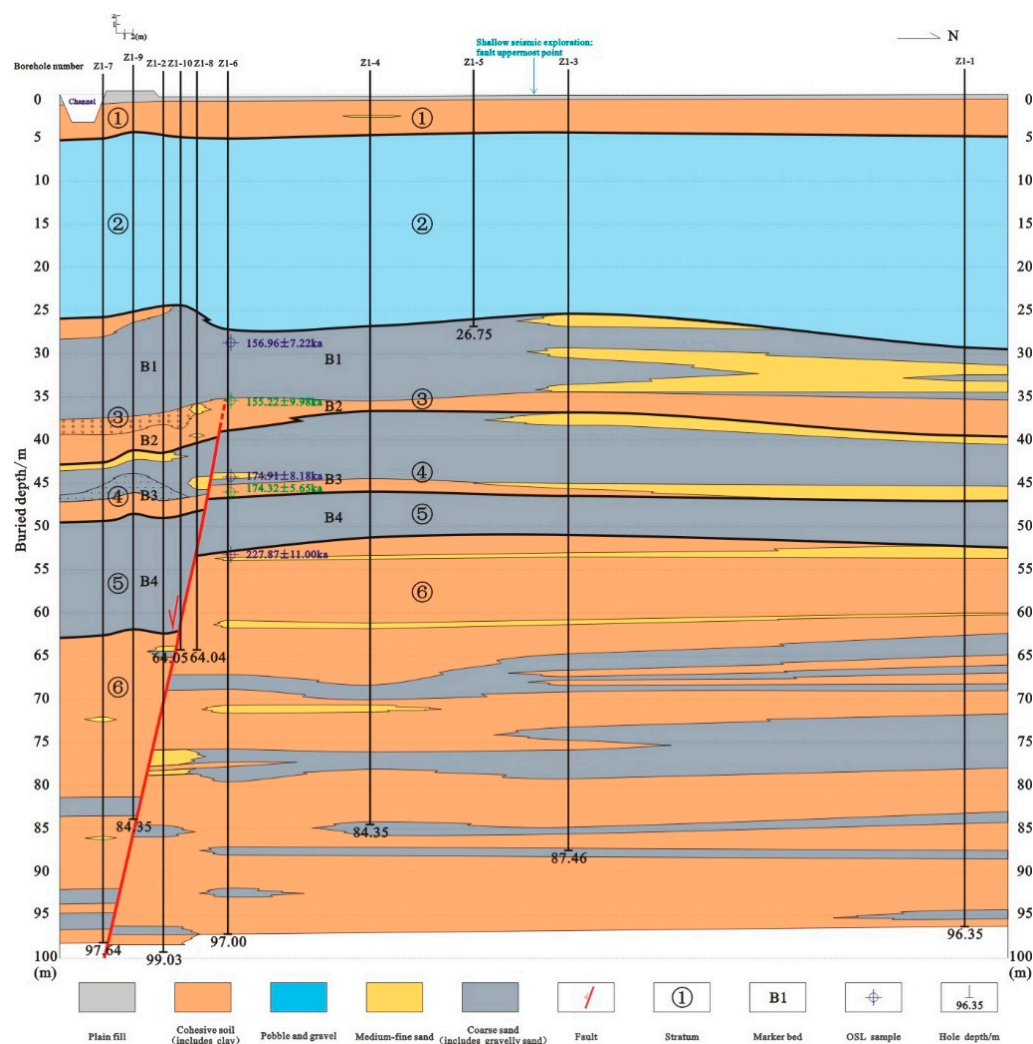
Figure 4. Stratigraphic lithology of composite drilling section in Xietan Village.

(1) The upper part of the Stratum ① is filled with earthy yellow plain fill, which contains plant roots and is moist and loose. The middle part consists of black-red and gray-white sandy clay, the bottom part has much sandy and is filled with light yellow clayey sand. This stratum is distributed 0~5 m below the Earth's surface and the sediment thickness is 4~5 m.

(2) The Stratum ② is a layer of variegated pebble and gravel, which is mainly gray-green and blue-green, followed by maroon and milky white. The pebble and gravel have fine psephicity. The maximum gravel diameter exceeds the drill core diameter by 10.8 cm. This stratum is distributed 5~30 m below the Earth's surface, its thickness decreases from north to south.

(3) The upper part of the Stratum ③ is light yellow with gravel-bearing coarse sand and gravelly sand. Some area is dark yellow or dark red. However, the upper parts of Z1-7, Z1-9 and Z1-2 have 1~3 m of dark red cohesive soil, silt and fine sand, its thickness decreases from north to south and finally thins out. The bottom parts of Z1-7, Z1-9, Z1-2 and Z1-10 gradually turn light red. The lower part is filled with light-red or dark-red cohesive soil and some areas have light red medium-fine sand. The bottom boundary of this stratum is different from the upper part of Stratum ④ in terms of gravelly sand's color and lithology. There is a dip of around 30° at the bottom boundary of Z1-2. This stratum is distributed 30~43 m below the Earth's surface; its thickness decreases from south to north.

(4) The upper part of Stratum ④ mainly consists of light-yellow gravelly sand, interbedded with medium-fine sand, medium-coarse sand or gravel-bearing coarse sand. The bottoms of Z1-8, Z1-4, Z1-3 and Z1-1 are black. The lower part of this stratum is light-red or dark-red cohesive soil sandwiched with thin layers of fine (silty) sand. The bottom boundary of Stratum ④ is obviously different from the light-yellow gravelly sand or light-yellow medium-fine sand in the upper part of Stratum ⑤ in color and lithology. The sandy clay interbedded with clay has a dip angle of about 20°. This stratum is distributed 43~50 m below the Earth's surface, thick in the middle and thin in the south and north sides.

(5) Stratum ⑤ mainly consists of light-yellow gravelly sand, with dark yellow mud in some areas. Its gravel content is between 25% and 50%, with poor sorting and psephicity. The maximum gravel diameter is about 8 cm. It has medium-fine sand, (medium) coarse sand and gravel-bearing coarse sand interbed. Its bottom boundary is significantly different from the light red/dark red clay soil in Stratum ⑥ in terms of color and lithology, making it easy to distinguish them. Z1-7, Z1-9, Z1-2 and Z1-10 are distributed 50~63 m below the Earth's surface and Z1-8, Z1-6, Z1-4, Z1-3 and Z1-1 are distributed 50~55 m below the Earth's surface. The thickness difference between the south and north of the stratum is large, which can be used as an obvious marker bed of fault dislocation.

(6) In Stratum ⑥, the light-red or dark-red cohesive soil layer, clay, clayey sand and sandy clay appear alternately. Some areas have black-red medium-coarse sand, gravel-bearing coarse sand or gravelly sand interbeds. The interbed is unstable in transverse contrast. Z1-7, Z1-9, Z1-2 and Z1-10 are distributed 63 m below the Earth's surface and Z1-8, Z1-6, Z1-4, Z1-3 and Z1-1 are distributed 55 m below the Earth's surface.

3.2.3. Marker Bed and Fault Location

During the composite drilling section exploration, the marker bed is the main basis for judging the fault location, fault displacement and the burial depth of the uppermost point. It has a stable horizon and its lithology and color are easily identified.

The composite drilling section in Xietan Village revealed four stable and comparable marker beds, which are used as the basis for studying the fault location and the burial depth of the uppermost point of the fault. The burial depth and thickness are shown in Table 2.

Table 2. The buried depth and thickness of marker beds revealed by composite drilling section in Xietan Village.

Marker Bed	Buried Depth and Thickness	Z1-7	Z1-9	Z1-2	Z1-10	Z1-8	Z1-6	Z1-4	Z1-3	Z1-1
B1	top boundary/m	27.50	26.83	25.35	24.15	26.29	26.93	26.63	25.29	29.31
	bottom boundary/m	38.06	37.86	36.54	36.48	35.51	34.92	35.28	33.50	35.27
	thickness/m	10.56	11.03	11.19	12.33	9.22	7.99	8.65	8.21	5.96
B2	top boundary/m	38.06	37.86	36.54	36.48	35.51	34.92	35.28	33.50	35.27
	bottom boundary/m	42.05	42.75	42.24	39.43	39.44	38.59	36.46	36.73	39.49
	thickness/m	3.99	4.89	5.70	2.95	3.93	3.67	1.18	3.23	4.22
B3	top boundary/m	42.05	42.75	42.24	39.43	39.44	38.59	36.46	36.73	39.49
	bottom boundary/m	48.81	48.95	48.72	47.62	47.41	46.42	45.77	46.41	45.66
	thickness/m	6.76	6.20	6.48	8.19	7.97	7.83	9.31	9.68	6.17
B4	top boundary/m	48.81	48.95	48.72	47.62	47.41	46.42	45.77	46.41	45.66
	bottom boundary/m	63.16	62.37	61.44	—	—	52.65	51.10	50.92	52.30
	thickness/m	14.35	13.42	12.72	—	—	6.23	5.33	4.51	6.64

Marker Bed B1 consists of light-yellow gravel-bearing coarse sand and gravelly sand. Some areas are dark yellow or dark red. Its gravel content is about 25%~50%, with poor sorting and psephicity. The maximum gravel diameter is around 8 cm. It has a thin layer compositing light yellow medium-fine sand or coarse sand. This marker layer is predominantly yellow, with coarse sand and gravelly sand as the main lithology. Its thickness ranges from 5.96~12.33 m, decreasing from south to north. The thickness of Z1-1 is only 5.96 m, which is probably due to the erosion of the upper pebble and gravel layer. The thickness of Z1-6 is 7.99 m, which is probably due to the deformation of the stratum by the lower fault. The thickness of the other drill holes is between 8.21~12.33 m.

Marker Bed B2 consists of light red/dark red cohesive soil, with a thin layer of light red medium-fine sand in some areas. The upper part of Z1-7, Z1-9, Z1-2 and Z1-10 has light red gravelly sand or gravel-bearing coarse sand. Given that the depositional environment in the same period is the same, it is appropriate to include them in this stratum. Its thickness is 2.95~5.70 m in the boreholes on the hanging wall of the fault and 1.18~4.22 m in the boreholes on the footwall of the fault. In general, the thickness of the hanging wall is greater than that of the footwall and the mark bed in Z1-8 and Z1-6 is (dark) black-red.

Stratum ④ is regarded as the Marker Bed B3, mainly due to the significant thickening of the light red/dark red cohesive soil layers in the lower part of Z1-7, Z1-9, Z1-2 and Z1-10 and little difference between the hanging wall and foot wall of B3's bottom boundary. Its thickness ranges from 6.17 m to 9.68 m in boreholes, increasing slightly from south to north. The boundary between the gravelly sand layer of Z1-8, Z1-6 and Z1-4 and cohesive soil is black. It can be taken as a typical feature of the same stratum and the footwall is slightly thicker than the hanging wall.

Marker Bed B4, i.e., Stratum ⑤, which is mainly light yellow and partially dark yellow, with distinct color and lithology. Its thickness ranges from 12.72 m to 14.35 m in the Z1-7, Z1-9 and Z1-2 on the hanging wall of the fault and from 4.51 to 6.64 m in Z1-6, Z1-4, Z1-3 and Z1-1 on the footwall of the fault. The hanging wall is thicker than the footwall, which facilitates the fault location.

The comparison results of the lithological column indicate that Marker Bed B1 is not broken. The top boundary of Marker Bed B2 is unbroken horizontally, while its bottom boundary is broken between Z1-8 and Z1-6. The bottom boundary of Marker Bed B3 is broken between Z1-8 and Z1-6. The fault is presumed to pass through the gravelly sand in Marker Bed B4 of the Z1-8 and the fault surface of this section is not preserved. In Z1-10, the fault may pass right through the boundary (60.80 m below the Earth's surface) between the gravelly sand and clayey sand. Only 63% of the cores were extracted due to abrasion of the gravels in the gravelly sands.

Taken together, the apparent dip of the fault is 78° and dips to the south. The uppermost point of the fault is buried at a depth of more than 35 m. The uppermost point is projected to the surface between Z1-8 and Z1-6, approximately 35 m to the south of the position identified by the shallow seismic exploration.

3.3. Sample Dating Test

The composite section exploration in Xietan Village is featured with clear strata and fault location. We selected five samples from the Z1-6 in the footwall of the fault. The dating results are shown in Table 3. As the dating results of OSL-08 and OSL-12 were inverted, we did not use them. The dating results of the other three samples are as follows: the OSL-05 with a buried depth of 28.43 m is (156.96 ± 7.22) ka BP; the OSL-11 with a buried depth of 44.00 m is (174.91 ± 8.18) ka BP; and the OSL-13 with a buried depth of 53.00 m is (227.87 ± 11.00) ka BP. According to the dating analysis of the above three samples, the age of middle-fine sand in the upper part of Stratum ③ (i.e., Marker Bed B1) below Stratum ② is (156.96 ± 7.22) ka BP. It is a reliable dating result, indicating that the stratum was deposited in the late Middle Pleistocene and was not broken by faults. The medium-fine sand in the lower part of Stratum 4 (i.e., Marker Bed B3) is (174.91 ± 8.18) ka BP, which was

deposited in the mid to late Middle Pleistocene and was broken by the fault. Therefore, the latest active period of the faults in Xietan Village was the middle-late Middle Pleistocene.

Table 3. The dating results of OSL samples in Xietan Village.

ID	Borehole Number	Lithology	Buried Depth/m	Age/ka
1	Z1-6	medium-fine sand	28.43	156.96 ± 7.22
2	Z1-6	clayey sand	35.15	155.22 ± 9.98
3	Z1-6	medium-fine sand	44.00	174.91 ± 8.18
4	Z1-6	clay	45.75	174.32 ± 5.65
5	Z1-6	clayey sand	53.00	227.87 ± 11.00

Active faults refer to faults that have been active for 120,000 years, including active faults in the Late Pleistocene and Holocene. In this regard, Hetan-Guotan buried fault is not an active fault because its last active period was the middle-late Middle Pleistocene and it became inactive at the end of Middle Pleistocene and has been since the Late Pleistocene.

4. Activity Characteristic of Zhenjing-Zhenbei Buried Fault

4.1. Shallow Seismic Exploration of Lizui Village's Survey Line

The shallow seismic exploration of Lizui Village's survey line (see Figure 2A) has revealed the existence of the Zhenjing-Zhenbei Buried Fault. Geophone interval of Lizui Village's survey line is 3 m, they extend from south to north with a total length of 3.0 km. To distinguish different reflected wave groups in the same time section and to facilitate interpretation, on the section map, we marked the bottom boundary reflection of the Quaternary overburden with T_Q and the bottom boundary reflection of the Neogene with T_N.

It can be seen from Figure 5a that the two-way travel time of the reflected wave is about 0.60 s, with rich seismic phases. In terms of the reflection characteristics, the preliminary interpretation results reveal that in the south of the survey line stake 1650 m from the starting point, the reflection event decreases significantly, only a few events can be tracked above 0.30 s and the transverse continuity of the events is poor. In the north of the survey line stake 1650 m from the starting point, the number of reflection events increases significantly and multiple sets of reflection events can be traced continuously. According to the characteristics of the reflected wave group and the faults on the section, there is a fault about 1650 m from the starting point. It is a normal fault dipping to the north and it breaks all stratigraphic reflections of the T_Q and the stratigraphic reflections below. The buried depth of the upper breakpoint is 73~80 m.

4.2. Composite Drilling Section Exploration in Lizui Village

4.2.1. Layout of Boreholes

Based on the shallow seismic exploration of Lizui Village's survey line, we took Lizui Village as a suitable site to perform the composite section exploration in Lizui Village. The specific site of the composite section exploration in Lizui Village is located in Zhenluo Town, east of Shapotou District, Zhongwei City (Figure 2A). The site is in the farmland 7 m east of the Lizui Village's survey line (Figure 2C). The SN direction of the section is nearly parallel to the Lizui Village's survey line. The boreholes intersected approximately vertically and crossed the Zhenjing-Zhenbei buried fault revealed by the shallow seismic exploration. The survey line of Lizui Village indicates that the uppermost point of the fault is 1650 m away from the starting point of the southern end and the fault is inclined to the north. The boreholes are arranged accordingly. The completed section is 113.6 m long, with 8 boreholes in total. The layout of boreholes is shown in Figures 2C and 5b. The maximum and minimum hole pitches are 44.0 m and 8.6 m, respectively, with an average hole pitch of 18.9 m (B is a Quaternary standard hole, 20 m north of Z2-7 and 0~100.60 m below the Earth's surface). The cumulative footage is 658.29 m and the maximum and minimum depths of a single borehole are 102.05 m and 85.33 m, respectively.
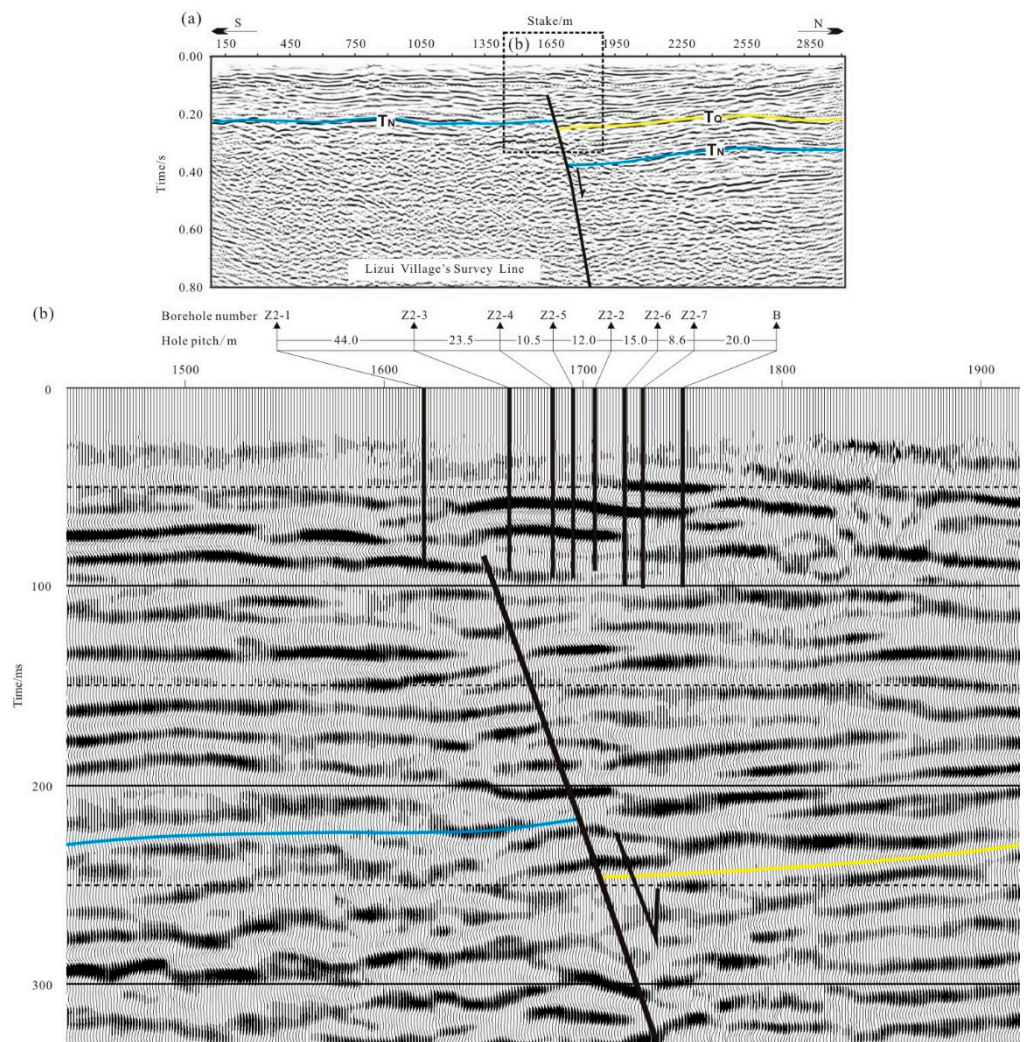
Figure 5. The time profile of Lizui Village's survey line and the layout of boreholes on composite drilling section in Lizui Village. (**a**) A time-stacked section of the shallow seismic line in Lizui Village. Dashed black box shows the location of (**b**). (**b**) The layout of boreholes on composite drilling section in Lizui Village.

4.2.2. Comparison of Stratigraphic Lithology

Based on the core logging of boreholes, we compared the lithological columns of each borehole and classified the stratigraphic lithology of the section of Lizui Village into seven strata (Figure 6 ①~⑦), which are described from top to bottom as follows:

(1) The surface layer of Stratum ① is filled with earthy yellow plain fill and the top boundary is the reconstruction surface of the farmland without height difference. The lower part is filled with greyish-yellow clayey sand and sandy clay with a greyish-black base due to the small amount of humus. This stratum is distributed 0~5 m below the Earth's surface and the sedimentary thickness varies slightly. It is 4.85 m thick in the south and gradually decreases to about 2.0 m in the north.

(2) Stratum ② is filled with variegated pebbles and gravels, which are mainly milky white, light red and greyish green, followed by dark gray and greyish black, with poor sorting and fine psephicity. The minimum gravel is 0.3~0.5 cm in diameter and the maximum gravel is 6.0~9.0 cm in diameter, with a complex composition and a thin layer of coarse sand of about 0.3 m. This stratum is distributed between 5 and 37 m below the Earth's surface. Its thickness decreases from south to north.

(3) In Stratum ③, the light red fine sand is interbedded with earthy yellow sandy clay, clayey sand and clay. It follows the sedimentary rhythm of fine sand-cohesive soil-fine sand-cohesive soil-fine sand-cohesive soil, with the exception that the light red fine sand at the top of Z2-1 thins out. This stratum is distributed between 37~48 m below the Earth's surface. It is slightly thin in the south and its thickness gradually increases from south to north. Its bottom boundary is 46~48 m below the Earth's surface.

(4) In Stratum ④, the light red fine sand is interbedded with earthy yellow (light red) sandy clay, clayey sand and clay. The upper part is a thick layer of light red fine sand interbedded with cohesive soil and the lower part is a cohesive soil layer interceded with light red fine sand. It follows the sedimentary rhythm of fine sand–cohesive soil– fine sand–cohesive soil–fine sand–cohesive soil. This stratum is distributed between about 48~60 m below the Earth's surface. It is slightly thick in the south and middle and slightly thin in the north.
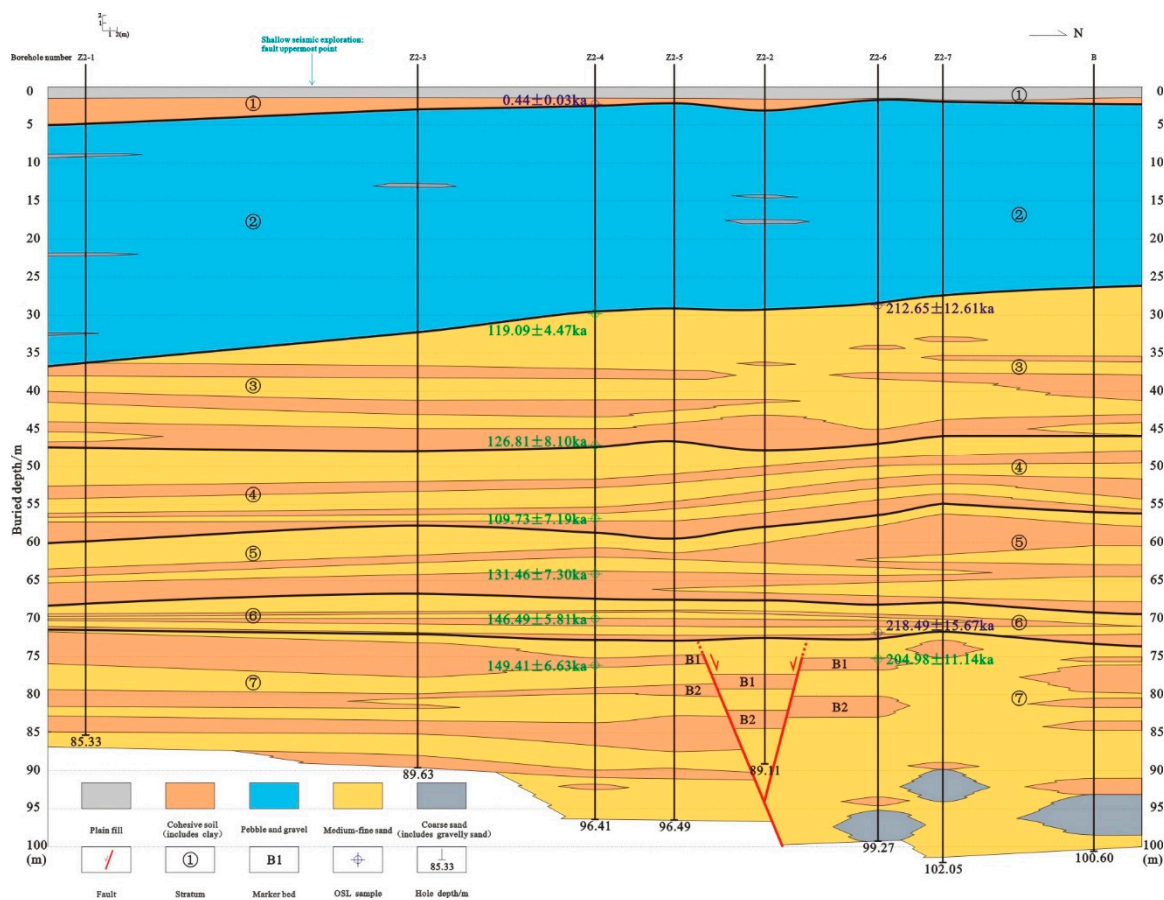

Figure 6. Stratigraphic lithology of composite drilling section in Lizui Village.

(5) Stratum ⑤ is filled with light red sandy clay, clayey sand, clay, fine sand or lenticular body. Z2-1, Z2-3 and Z2-4 have fine sand sandwiched with cohesive soil in the upper part and cohesive soil interbedded with fine sand in the lower part, following the sedimentary rhythm of fine sand-cohesive soil-fine sand-cohesive soil. The upper part of Z2-5, Z2-2, Z2-6 and Z2-7 is the same as that of Z2-1, Z2-3 and Z2-4, but Z2-5, Z2-2, Z2-6 and Z2-7 have a fine sand lenticular body and sand agglomerates in the lower part. This stratum is distributed between about 60~68 m below the Earth's surface It is slightly thick in the south and its thickness gradually increases from south to north.

(6) In Stratum ⑥, the light red fine sand is interbedded with sandy clay, clayey sand and clay. It is mainly filled with light red fine sand. There are many sandy agglomerates. This stratum is distributed between about 68~73 m below the Earth's surface. The thickness of the stratum is stable. The middle is slightly thick and the sides are thin.

(7)　Stratum ⑦ is a layer composed of light red fine sand interbedded with earthy yellow (light red) cohesive soil. Part of Z2-6, Z2-7 and B have pebbles and gray-black gravel-bearing coarse sand. This stratum is distributed 73 m below the Earth's surface.

4.2.3. Marker Bed and Fault Location

The marker bed refers to the same stratum that is continuously distributed in the section and is significantly different from the upper and lower strata. The cohesive soil (including clay, clayey sand and sandy clay) in the fluvial strata of Zhongwei Basin is generated under weak hydrodynamic force and a stable depositional environment. It is hard with a high and reliable core recovery percentage. Therefore, we selected a cohesive soil layer with a certain thickness and stable distribution as the marker bed.

We figured out the location of the fault of the composite drilling section in Lizui Village by locating two obvious marker beds in Stratum ⑦ (Table 4). The brief introduction is as follows:

Table 4. The buried depth and thickness of Stratum ⑥ and marker beds revealed by composite drilling section in Lizui Village.

Marker Bed	Buried Depth and Thickness	Z2-1	Z2-3	Z2-4	Z2-5	Z2-2	Z2-6	Z2-7	B
Stratum ⑥	top boundary/m	68.10	66.75	67.41	67.53	67.61	68.22	67.66	69.22
	bottom boundary/m	71.50	72.05	72.83	72.91	72.56	72.65	71.01	73.17
	thickness/m	3.40	5.30	5.42	5.38	4.95	4.43	3.35	3.95
B1	top boundary/m	71.84	73.18	75.21	74.79	77.30	75.14	—	—
	bottom boundary/m	76.14	77.70	76.40	76.09	79.24	76.75	—	—
	thickness/m	4.30	4.52	1.19	1.30	1.94	1.61	—	—
B2	top boundary/m	79.38	79.89	79.16	78.71	82.07	80.17	—	—
	bottom boundary/m	81.54	81.82	79.87	80.13	84.47	82.44	—	—
	thickness/m	2.16	1.93	0.71	1.42	2.40	2.27	—	—

Marker Bed B1 mainly consists of light red sandy clay and clay. Some areas have a thin layer of clayey sand. The thickness of Z2-1 and Z2-3 is between 4.30 to 4.52 m and the thickness of Z2-4 and Z2-5 near the footwall of the fault is 1.19~1.30 m. This marker bed of Z2-2 in the hanging wall of fault drops by about 3.0 m and its thickness increases slightly. Z2-6 is about 2.0 m higher than Z2-2, but about 0.5 m lower than Z2-5.

Marker Bed B2 mainly consists of light red clay, with thin layers of sandy clay and fine sand in some areas. Z2-1 and Z2-3 are thick, ranging from 1.93 m to 2.16 m, while Z2-4 and Z2-5 near the footwall of the fault are thin, ranging from 0.71 m to 1.42 m. This marker bed of Z2-2 in the hanging wall of fault drops by about 4.0 m and its thickness increases significantly. Z2-6 is about 3.0 m higher than Z2-2, but about 1.5 m lower than Z2-5.

The stratigraphic comparison shows that the bottom boundary of Stratum ⑥ (the top boundary of Stratum ⑦) is not broken and overlaid on the fault. The two marker beds in Stratum ⑦ are broken and reverse faults are developed. The main fault is located between Z2-5 and Z2-2 and the reverse secondary fault is located between Z2-2 and Z2-6. The marker beds of Z2-2 descends and thickens, indicating that the fault is normal. According to Table 3, the bottom boundary of Stratum ⑥ is 71.01~72.91 m, so the position of the uppermost point of the fault is not higher than 71 m.

Taken together, the apparent dip of the main fault is 67° and the normal fault dips to the north. The uppermost point of the fault is buried at a depth of more than 71 m. The uppermost point is projected to the surface between Z2-5 and Z2-2, approximately 50 m to the north of the position identified by the shallow seismic exploration.

4.3. Sample Dating Test

Ten samples from Z2-4 and Z2-6 were selected. A few samples showed inverted assay results, but it did not affect the sequence determination of the overall stratigraphic depositional age. Table 5 shows the dating results of the samples. It can be seen that the ages of samples from Z2-6 are older than those from Z2-4 overall, especially the ages of samples under the pebble and gravel layer. The ages of samples from Z2-4 are between (109.73 ± 7.19) to (149.41 ± 6.63) ka BP, while those from Z2-6 are between (204.98 ± 11.14) to (218.49 ± 15.67) ka BP. These ages are close to the maximum age measured by the Optically Stimulated Luminescence dating and the actual stratigraphic age may be older than the dating results. Moreover, the age of Z2-4 varies by only about 40 ka from 29.79 m to 76.15 m below the Earth's surface and that of Z2-6 varies by only about 10 ka from 28.68 m to 75.29 m below the Earth's surface, which is quite unreasonable. We deem that the sedimentary strata 71 m below the Earth's surface were likely to be formed in the Early Pleistocene; thus, the main fault activity is presumed to happen in the Early to Middle Pleistocene.

Table 5. The dating results of OSL samples in Lizui Village.

ID	Borehole Number	Lithology	Buried Depth/m	Age/ka
1	Z2-4	clayey sand	2.26	0.44 ± 0.03
2	Z2-4	fine sand	29.79	119.09 ± 4.47
3	Z2-4	clay	47.11	126.81 ± 8.10
4	Z2-4	clay	56.86	109.73 ± 7.19
5	Z2-4	clay	64.15	131.46 ± 7.30
6	Z2-4	sandy clay	70.04	146.49 ± 5.81
7	Z2-4	clayey sand	76.15	149.41 ± 6.63
8	Z2-6	fine sand	28.68	212.65 ± 12.61
9	Z2-6	fine sand	71.84	218.49 ± 15.67
10	Z2-6	clay	75.29	204.98 ± 11.14

According to the definition of an active fault, Zhenjing-Zhenbei buried fault is not an active fault because its latest active period was the Early and Middle Pleistocene and it has been inactive at the end of Middle Pleistocene and since the Late Pleistocene.

5. Discussion

5.1. Relationship between Two Buried Faults and Tianjingshan Fault

The Hetan-Guotan buried fault and the Zhenjing-Zhenbei buried fault are located in the Zhongwei Basin, while Tianjingshan Fault is the southern boundary of the Zhongwei Basin [24]. According to the latest research results of regional tectonic, Zhongwei Basin is mainly controlled by the Tianjingshan Fault, an arc fault that has been strongly active since the late Pleistocene in the northeastern margins of Tibetan Plateau [25–27]. The arcuate tectonic belt on the northeastern margins of Tibetan Plateau has been gradually pushed outward through the subsidiary block. The Tianjingshan Fault experienced two stages of tectonic evolution in the late Cenozoic. The early Xiangshan-Tianjingshan block was pushed to move northeastwards, making the Tianjingshan Fault a thrust fault. The late Xiangshan-Tianjingshan block was blocked in its north-easterly movement and moved to the east, where the blocking effect was weak, making the Tianjingshan Fault a strike-slip fault. The strike-slip displacement is absorbed by the extensional tectonic at the southeast end of the fault. The thrust might start at the Early Pliocene, i.e., 5.4 Ma, and the sinistral strike-slip motion might start at the end of Pliocene, i.e., 2.6 Ma [28,29]. Since the Pleistocene, the SEE Tianjingshan Fault in the south of Zhongwei Basin has moved in the form of a thrust-sinistral strike-slip fault. The two buried faults might be affected by the activity of Tianjingshan Fault. Due to the large scale and strong activity of Tianjingshan Fault, the regional strike-slip deformation is mainly concentrated in the south of Zhongwei Basin. As

a result, the two buried faults were weakly active in the Early and Middle Pleistocene until they ceased to be active in the Late Pleistocene.

5.2. Seismic Hazard Assessment of Two Buried Faults in the Zhongwei Basin

Zhongwei City, located in the Zhongwei Basin, has a permanent population of 402,000. This study fills the gap in the detection of active faults in Zhongwei City. The results show that the Hetan-Guotan buried fault and the Zhenjing-Zhenbei buried fault are small in scale, measuring 12.5 km and 8.8 km, respectively. They were inactive since the Late Pleistocene. Therefore, it is concluded that the two buried faults do not present the conditions for destructive earthquakes in the future. Although there are some small, scattered earthquakes in Zhongwei Basin, they are not associated with the large arc-shaped structural zones, which is a local regulation. Presumably, the two buried faults will be dominated by small earthquake activity in the future. It is highly unlikely that they will threaten the urban security of Zhongwei City.

6. Conclusions

(1) Based on the survey line of shallow seismic exploration in Xietan Village, the composite drilling section in Xietan Village revealed that the exact location of the Hetan-Guotan buried fault is approximately 35 m to the south of the position identified by the shallow seismic exploration of Xietan Village's survey line, with an apparent dip of 78°. Moreover, the burial depth of the uppermost point is 35 m. According to the dating test results of the samples, we found that its latest activity period was the mid-late Middle Pleistocene and it was inactive at the end of Middle Pleistocene and since the Late Pleistocene; thus, it is not an active fault.

(2) According to the survey line of shallow seismic exploration in Lizui Village, the composite drilling section in Lizui Village revealed that the exact location of the Zhenjing-Zhenbei buried fault is about 50 m to the north of the position identified by the shallow seismic exploration of Lizui Village's survey line, with an apparent dip of 67°. Moreover, the burial depth of the uppermost point is 71 m. According to the dating test results of the samples, we found that its latest activity period was the Early and Middle Pleistocene, and it was inactive at the end Middle Pleistocene and since the Late Pleistocene; thus, it too is not an active fault.

(3) Influenced by the activity of Tianjingshan Fault, the Hetan-Guotan buried fault and the Zhenjing-Zhenbei buried fault were weakly active in the Early and Middle Pleistocene until they ceased to be active in the Late Pleistocene. Due to the large scale and strong activity of Tianjingshan Fault, the regional strike-slip deformation is mainly concentrated in the south of Zhongwei Basin. The two buried faults are small in scale, measuring 12.5 km and 8.8 km, respectively. It is concluded that the two buried faults do not present the conditions for destructive earthquakes in the future. Presumably, the two buried faults will be dominated by small earthquake activity in the future. It is highly unlikely that they would have threatened the urban security of Zhongwei City.

Author Contributions: Data curation, C.L.; Formal analysis, C.L. and Q.L.; Methodology, C.L. and Q.L.; Project administration, Q.L.; Supervision, P.D.; Validation, Z.W., Z.L., S.Y. (Sihan Yu), S.Y. (Shun Yang) and Y.W.; Formal analysis, C.L., Q.L.; Investigation, C.L., Z.W. and Z.L.; Resources, P.D., Z.W., Z.L., S.Y. (Sihan Yu), S.Y. (Shun Yang) and Y.W.; Writing—original draft, C.L.; Writing—review & editing, Q.L. and P.D.; Visualization, S.Y. (Sihan Yu), S.Y. (Shun Yang) and Y.W. All authors have read and agreed to the published version of the manuscript.

Institutional Review Board Statement: Not applicable.

Informed Consent Statement: Not applicable.

Data Availability Statement: The data used to support the findings of this study are included within the article.

Conflicts of Interest: The authors declare that they have no conflict of interest.

References

1. Middleton, T.A.; Walker, R.T.; Parsons, B.; Lei, Q.Y.; Zhou, Y.; Ren, Z.K. A major, intraplate, normal-faulting earthquake: The 1739 Yinchuan event in northern China. *J. Geophys. Res. Solid Earth* **2016**, *121*, 293–320. [CrossRef]
2. Butler, R.; Stewart, G.S.; Kanamori, H. The 27 July 1976 Tangshan, China earthquake—A complex sequence of intraplate events. *Bull. Seismol. Soc. Am.* **1979**, *69*, 207–220. [CrossRef]
3. Hearn, E.; Mcclusky, S.; Ergintav, S.; Reilinger, R.E. Izmit earthquake postseismic deformation and dynamics of the North Anatolian Fault Zone. *J. Geophys. Res. Solid Earth* **2009**, *114*, 1621–1643. [CrossRef]
4. Deng, Q.D. Exploration of active faults and their seismic hazard assessments. *Seismol. Geol.* **2002**, *24*, 601–605.
5. Zhang, P.Z.; Deng, Q.D.; Zhang, Z.Q.; Li, H.B. Active fault, earthquake disaster in China and its dynamic process. *Sci. China Ser. D Earth Sci.* **2013**, *43*, 1607–1620.
6. King, C. Radon emanation on San Andreas Fault. *Nature* **1978**, *271*, 516–518. [CrossRef]
7. Ciotoli, G.; Etiope, G.; Guerra, M.; Lombardi, S. The detection of concealed faults in the Ofanto Basin using the correlation between soil-gas fracture surveys. *Tectonophysics* **1999**, *301*, 321–332. [CrossRef]
8. Etiope, G.; Guerra, M.; Raschi, A. Carbon dioxide and radon geohazards over a gas-bearing fault in the Siena Graben (Central Italy). Terrestrial Atmospheric and Oceanic. *Sciences* **2005**, *16*, 885–896.
9. Fuis, G.; Ryberg, T.; Lutter, W.; Ehlig, P. Seismic mapping of shallow fault zones in the San Gabriel Mountains from the Los Angeles Region Seismic Experiment, southern California. *J. Geophys. Res. Solid Earth* **2001**, *106*, 6549–6568. [CrossRef]
10. Wyatt, D.; Waddell, M.; Sexton, G. Geophysics and shallow faults in unconsolidated sediments. *Groundwater* **2010**, *34*, 326–334. [CrossRef]
11. Chai, C.Z.; Meng, G.K.; Du, P.; Wang, Y.; Liu, B.J.; Shen, W.H.; Lei, Q.Y.; Liao, Y.H.; Zhao, C.B.; Feng, S.Y.; et al. Comprehensive multi-level exploration of buried active fault: An example of Yinchuan buried active fault. *Seismol. Geol.* **2006**, *28*, 536–544.
12. Pratt, T.L.; Shaw, J.H.; Dolan, J.F.; Christofferson, S.A.; Williams, R.A.; Odum, J.K.; Plesch, A. Shallow seismic imaging of folds above the Puente Hills blind-thrust fault, Los Angeles, California. *Geophys. Res. Lett.* **2002**, *29*, 18-1–18-4. [CrossRef]
13. Liu, B.J.; Chai, C.Z.; Feng, S.Y.; Zhao, C.B.; Yuan, H.K. Seismic exploration method for buried fault and its up-breakpoint in Quaternary sediment area—An example of Yinchuan buried active fault. *Chin. J. Geophys.* **2008**, *51*, 1475–1483. [CrossRef]
14. Pugin, A.J.M.; Pullan, S.E.; Hunter, J.A.; Oldenborger, G.A. Hydrogeological prospecting using P- and S-wave landstreamer seismic reflection methods. *Near Surf. Geophys.* **2009**, *7*, 315–327. [CrossRef]
15. Malehmir, A.; Dahlin, P.; Lundberg, E.; Juhlin, C.; Sjöström, H.; Högdahl, K. Reflection seismic investigations in the Dannemora area, central Sweden: Insights into the geometry of polyphaser deformation zones and magnetite-skarn deposits. *J. Geophys. Res.* **2011**, *116*, B11307. [CrossRef]
16. Brodic, B.; Malehmir, A.; Junlin, C.; Dynesius, L.; Bastani, M.; Palm, H. Multicomponent broadband digital-based seismic landstreamer for near-surface applications. *J. Appl. Geophys.* **2015**, *123*, 227–241. [CrossRef]
17. Lei, Q.Y.; Chai, C.Z.; Meng, G.K.; Du, P.; Wang, Y.; Xie, X.F.; Zhang, X.H. Composite drilling section exploration of Yinchuan buried fault. *Seismol. Geol.* **2008**, *30*, 250–262.
18. Zhang, S.M.; Wang, D.D.; Liu, X.D.; Zhang, G.H.; Zhao, J.X.; Luo, M.H.; Ren, J.J.; Wang, R.; Zhang, Y.L. Using borehole core analysis to reveal late Quaternary paleoearthquakes along the Nankou-Sunhe Fault, Beijing. *Sci. China Ser. D Earth Sci.* **2008**, *38*, 881–895. [CrossRef]
19. Liang, K.; Sun, C.B.; Ma, B.Q.; Tian, Q.J.; Li, D.W.; Li, D.W.; He, Z.T. Investigation of the Yellow River buried fault in the Wuhai basin, northwestern Ordos Block, China, using deep/shallow seismic reflection and drilling techniques. *J. Asian Earth Sci.* **2018**, *163*, 54–69. [CrossRef]
20. Tapponnier, P.; Molnar, P. Active faulting and Cenozoic tectonics of China. *J. Geophys. Res.* **1977**, *82*, 2905–2930. [CrossRef]
21. Zhang, P.Z.; Burchfiel, B.C.; Molnar, P.; Zhang, W.Q.; Jiao, D.C.; Deng, Q.D.; Wang, Y.P.; Royden, L.; Song, F.M. Late Cenozoic tectonic evolution of the Ningxia-Hui autonomous region, China. *Geol. Soc. Am. Bull.* **1990**, *102*, 1484–1498.
22. Li, X.N.; Li, C.Y.; Wesnousky, S.G.; Zhang, P.Z.; Zheng, W.J.; Pierce, I.K.D.; Wang, X.G. Paleoseismology and slip rate of the western Tianjingshan fault of NE Tibet, China. *J. Asian Earth Sci.* **2017**, *146*, 304–316. [CrossRef]
23. Lei, Q.Y.; Chai, C.Z.; Meng, G.K.; Du, P.; Wang, Y.; Xie, X.F. Method of locating buried active fault by composite drilling section doubling exploration. *Seismol. Geol.* **2011**, *33*, 45–55.
24. Zhang, K.; Liu, K.Y.; Wu, J.M.; Yang, J.C.; Cai, J.B. Depositional features of the Zhongwei Basin, Ningxia, and its implications for Neotectonic movements. *Acta Sedimentol. Sin.* **2004**, *22*, 465–473.
25. Zhang, W.Q.; Jiao, D.C.; Chai, C.Z. *The Tianjingshan Active Fault Zone*; Seismological Press: Beijing, China, 2015; pp. 140–153.
26. Li, X.N.; Li, C.Y.; Zhang, P.Z.; Wang, X.G.; Zhang, L.S. Changes in fault movement property and genetic machanism on the western segment of the Xiangshan-Tianjingshan fault zone. *Seismol. Geol.* **2016**, *38*, 732–746.

27. Dong, J.Y.; Luo, Q.X.; Li, X.N.; Li, C.Y.; Yang, H.L.; Ren, G.H. Determination and Spatial Pattern of the Late Quaternary Left-lateral Slip Rate of the Tianjingshan Fault. *Acta Geosci. Sin.* **2021**, *42*, 527–536.

28. Wang, W.T.; Zhang, P.Z.; Kirby, E.; Wang, L.H.; Zhang, G.L.; Zheng, D.W.; Chai, C.Z. A revised chronology for Tertiary sedimentation in the Sikouzi Basin: Implications for the tectonic evolution of the northeastern corner of the Tibetan plateau. *Tectonophysics* **2011**, *505*, 100–114. [CrossRef]

29. Lei, Q.Y.; Zhang, P.Z.; Zheng, W.J.; Chai, C.Z.; Wang, W.T.; Du, P.; Yu, J.X. Dextral strike-slip of Sanguankou-Niushoushan fault zone and extension of arc tectonic belt in the northeastern margin of the Tibet Plateau. *Sci. China Ser. D Earth Sci.* **2016**, *46*, 691–705. [CrossRef]